Development 133, 3859-3870 (2006) doi:10.1242/dev.02555

General and cell-type specific mechanisms target TRPP2/PKD-2 to cilia

Young-Kyung Bae[1,2], Hongmin Qin[3,*], Karla M. Knobel[2], Jinghua Hu[2], Joel L. Rosenbaum[3] and Maureen M. Barr[2,†]

Ciliary localization of the transient receptor potential polycystin 2 channel (TRPP2/PKD-2) is evolutionarily conserved, but how TRPP2 is targeted to cilia is not known. In this study, we characterize the motility and localization of PKD-2, a TRPP2 homolog, in *C. elegans* sensory neurons. We demonstrate that GFP-tagged PKD-2 moves bidirectionally in the dendritic compartment. Furthermore, we show a requirement for different molecules in regulating the ciliary localization of PKD-2. PKD-2 is directed to moving dendritic particles by the UNC-101/adaptor protein 1 (AP-1) complex. When expressed in non-native neurons, PKD-2 remains in cell bodies and is not observed in dendrites or cilia, indicating that cell-type specific factors are required for directing PKD-2 to the dendrite. PKD-2 stabilization in cilia and cell bodies requires LOV-1, a functional partner and a TRPP1 homolog. In *lov-1* mutants, PKD-2 is greatly reduced in cilia and forms abnormal aggregates in neuronal cell bodies. Intraflagellar transport (IFT) is not essential for PKD-2 dendritic motility or access to the cilium, but may regulate PKD-2 ciliary abundance. We propose that both general and cell-type-specific factors govern TRPP2/PKD-2 subcellular distribution by forming at least two steps involving somatodendritic and ciliary sorting decisions.

KEY WORDS: Autosomal Dominant Polycystic Kidney Disease, *C. elegans*, TRPP2 (PKD2)/PKD-2

INTRODUCTION

Autosomal dominant polycystic kidney disease (ADPKD) is the most common monogenic disease, affecting one in 800 individuals (Igarashi and Somlo, 2002). In individuals with ADPKD, the kidneys accumulate multiple cysts that ultimately cause end-stage renal disease. Mutation in the *PKD1* or *PKD2* gene accounts for 95% of ADPKD cases (Hughes et al., 1995; Mochizuki et al., 1996). *PKD1* and *PKD2* encode a large 11-transmembrane spanning receptor (TRP polycystin 1, TRPP1) and transient receptor potential channel (TRP polycystin 2, TRPP2), respectively (Clapham, 2003). Mammalian TRPP1 and TRPP2 (PKD2 – Mouse Genome Informatics) localize to primary cilia of kidney epithelial cells (Pazour et al., 2002; Yoder et al., 2002), where they function in a mechanosensory capacity (Nauli et al., 2003). ADPKD is one of a number of human genetic diseases that are rooted in defects in cilia formation, maintenance, or function (Pazour, 2004; Pazour and Rosenbaum, 2002; Watnick and Germino, 2003). Understanding the mechanisms by which TRPP1 and TRPP2 are transported to and function in cilia is important from both the basic cell biology and human health perspectives.

The nematode *Caenorhabditis elegans* is a powerful model system with which to understand how cilia form and function. *C. elegans* polycystins TRPP1/LOV-1 and TRPP2/PKD-2 localize on the ciliary membrane and are required for male sensory behaviors (Barr et al., 2001; Barr and Sternberg, 1999). Hence, the connection between the polycystins and cilia seems to be an ancient one. Moreover, many *C. elegans* proteins that are required for formation, maintenance and function of cilia are linked to human renal diseases, including ADPKD, Bardet-Biedl Syndrome (BBS) and nephronophthisis (Barr, 2005).

PKD-2 is a member of the evolutionarily conserved TRP ion channel superfamily and acts in the same genetic pathway with LOV-1. In male-specific ciliated sensory neurons, PKD-2 and LOV-1 are required for two mating behaviors – response to mate contact and location of the mate's vulva – and are postulated to sense cues from the mate. TRP channels function as sensory receptors of diverse stimuli (Clapham, 2003). TRP vanilloid (TRPV) channels localize to cilia in mammals, *Drosophila*, and the nematode (Andrade et al., 2005; Colbert et al., 1997; Kim et al., 2003). In *C. elegans*, the TRPV channels OSM-9 and OCR-2 are mutually dependent on each other for ciliary localization and sensory function (Tobin et al., 2002). In *Drosophila*, the ciliary localization of TRPV hearing channels Nanchung (NAN) and Inactive (IAV) is also co-dependent (Gong et al., 2004). Human TRPP1 has been implicated in transporting TRPP2 from ER to plasma membrane (Hanaoka et al., 2000). A recent study found that TRPP2 localizes to cilia independently of TRPP1 in LLC-PK1 and MDCK epithelial cells (Geng et al., 2006), while another shows that TRPP2 ciliary localization is dependent of TRPP1 in collecting duct-derived epithelial cells (Nauli et al., 2003).

Intraflagellar transport (IFT) is a motility process required for the assembly and maintenance of cilia and flagella (Rosenbaum and Witman, 2002) and defects in IFT may result in PKD (Pazour and Rosenbaum, 2002). IFT is required for the ciliary movement of axonemal structural components, the IFT machinery itself, and the membrane-bound sensory receptors OSM-9 and OCR-2 (Kozminski et al., 1995; Kozminski et al., 1993; Orozco et al., 1999; Qin et al., 2005; Qin et al., 2004; Snow et al., 2004). PKD-2 motility in cilia is not detected, suggesting that PKD-2 may diffuse into the ciliary membrane, that PKD-2 may be physically restrained at the cilium, or that at least two mechanisms regulate ciliary protein localization (Peden and Barr, 2005; Qin et al., 2005). In *C. elegans* and mammals, IFT does not appear to be essential for membrane

[1]Laboratory of Genetics and [2]School of Pharmacy, Division of Pharmaceutical Sciences, University of Wisconsin-Madison, Madison, WI 53705-2222, USA. [3]Department of Molecular, Cellular and Developmental Biology, Yale University, New Haven, CT 06511, USA.

*Present address: Department of Biology, Texas A&M University, College Station, TX 77843, USA
†Author for correspondence (e-mail: mmbarr@pharmacy.wisc.edu)

Accepted 27 July 2006

receptor transport into cilia but may regulate ciliary membrane protein abundance (Pazour et al., 2002; Qin et al., 2005; Qin et al., 2001).

Dynamic regulation of receptor localization is a common theme in signaling pathways. We previously reported that ciliary localization of *C. elegans* PKD-2 is modulated by its phosphorylation status (Hu et al., 2006). Casein kinase 2 (CK2) and the TAX-6 calcineurin phosphatase regulate PKD-2 function and ciliary abundance, but not the initial targeting of PKD-2 to cilia. PKD-2 ciliary abundance is regulated also by KLP-6, a cell-type specific kinesin 3 (Peden and Barr, 2005). KLP-6 is not essential for ciliogenesis or for PKD-2 entrance to cilia. However, PKD-2::GFP accumulates in the ciliary base and cilium in a *klp-6* mutant. KLP-6 has been proposed to act as an anchor to tether PKD-2 between the ciliary membrane and microtubule axoneme or to act redundantly with the IFT machinery.

TRPP1 and TRPP2 must ultimately be localized to cilia in order to conduct the sensory function of the cell, whether it is a human renal epithelial cell or a worm sensory neuron. How TRPP1, TRPP2 and other ciliary proteins localize and gain access to the cilium, a spatially restricted organelle, is not well understood. After proper entrance to the cilium, regulation of PKD-2 ciliary abundance may be an equally important step for its sensory function. Given that it is prohibitively difficult to study TRPP2 ciliary localization in humans, we exploited the transparency of *C. elegans* and took a genetic approach to uncover the mechanisms governing PKD-2 localization in living animals. PKD-2 bidirectional motility rates in dendrites of male-specific sensory neurons is comparable with that of the olfactory G protein-coupled receptor ODR-10 in dendrites of chemosensory AWB amphid neurons (Dwyer et al., 2001; Sengupta et al., 1996), suggesting that a common dendritic transport machinery acts in diverse cell types. By analyzing candidate trafficking mutants, we show that PKD-2 subcellular localization requires two sorting steps. The somatodendritic sorting step acts between the neuronal cell body and dendrite, while the ciliary sorting step acts between the distal dendrite and cilium to regulate PKD-2 ciliary localization and abundance.

MATERIALS AND METHODS

C. elegans strains

Nematodes were raised using standard conditions (Brenner, 1974). Strains used for injections were: 'wild type', *him-5(e1490)V* (Hodgkin, 1983) and *pha-1(e2123ts)III; him-5(e1490)V* (Granato et al., 1994). A categorized *C. elegans* strain list follows.

General

CB1490, *him-5(e1490)V; PS2172, pha-1(e2123ts)III; him-5(e1490)V*; PT9, *pkd-2(sy606)IV; him-5(e1490)V*; PT572, *myIs1[PKD-2::GFP; cc:GFP] pkd-2(sy606)IV; him-5(e1490)V*; PT573, *myIs1 IV; him-5(e1490)V*; PT618, *pkd-2(sy606)IV; myIs4[PKD-2::GFP; cc::GFP] him-5(e1490)V*; PT621, *myIs4 him-5(e1490)V*.

unc-101 and *lov-1* mutants

PT624, *unc-101(m1)I; pkd-2(sy606)IV; myIs4 him-5(e1490) V*; PT657, *lov-1(sy582)II; myIs4 him-5(e1490)V*; PT658, *lov-1(sy582)II; pkd-2(sy606)IV; myIs4 him-5(e1490)V*; PT970, *unc-101(m1)I; lov-1(sy582)II; myIs4 him-5(e1490)V.*

IFT mutants

PT628, *osm-3(p802) pkd-2(sy606)IV; myIs4 him-5(e1490)V*; PT629, *pkd-2(sy606)IV; myIs4 him-5(e1490)V; osm-5(m184)X*; PT630, *che-13(e1805)I; pkd-2(sy606)IV; myIs4 him-5(e1490)V*; PT631, *daf-10(p821)IV; myIs4 him-5(e1490)V*; PT677, *che-13(e1805)I; daf-10(p821)IV; myIs4 him-5(e1490)V*; PT678, *daf-10(p821)IV; myIs4 him-5(e1490)V; osm-5(m184)X*; PT632, *che-3(e1124)I; myIs4 him-5(e1490)V*; PT633, *klp-11(tm324)IV; myIs4 him-5(e1490)V*; PT868, *kap-1(ok676) III; klp-11(tm324) IV; myIs4 him-5(e1490)V*; PT870, *kap-1(ok676) III; myIs4 him-5(e1490)V*; PT1184, *osm-12(n1606) III; myIs4 him-5(e1490)V.*

ER markers

PT665, *pha-1(e2123ts)III; him-5(e1490) myEx342[Ppkd-2::GFP::KDEL; pBX]*; PT977, *pha-1(e2123ts)III; him-5(e1490) V myEx469[Ppkd-2::TRAM::GFP; pBX]*; PT1126, *pha-1(e2123ts)III; myIs4 him-5(e1490) V myEx500[Ppkd-2::TRAM::DsRed2; pBX].*

TBB-4 markers

PT1018, *pha-1(e2123ts)III; him-5(e1490) V myEx481[Ppkd-2::TBB-4::DsRed2; pBX]*; PT1020, *pha-1(e2123ts)III;osm-3(p802) IV; myIs4 him-5(e1490)V myEx481*; PT1022, *pha-1(e2123ts)III; myIs4 him-5(e1490) V osm-5(m184)X myEx481*; PT1024, *che-3(e1184)I; pha-1(e2123ts)III; myIs4 him-5(e1490) V myEx481*; PT1026, *pha-1(e2123ts)III; klp-11(tm324)IV; myIs4 him-5(e1490)V myEx481.*

Strains for pan-neuronal expression of PKD-2::GFP

PT1027, *pha-1(e2123ts)III; him-5(e1490) V; myEx482[Punc-119::PKD-2::GFP; pBX]*; PT1028, *unc-101(m1)I; pha-1(e2123ts)III; him-5(e1490)V myEx482*; PT1029, *pha-1(e2123ts)III; lov-1(sy582)IV; him-5(e1490)V myEx482.*

Strains for co-expression of Kinesin II *kap-1* with *pkd-2*

PT1030, *pha-1(e2123ts)III; him-5(e1490) V myEx508[KAP-1::GFP; Ppkd-2::DsRed2; pBX].*

pkd-2 cDNA and promoter identification

The 5′ transcriptional initiation site of *pkd-2* was identified using 5′ RACE (Roche). A full-length *pkd-2* cDNA was generated by PCR, subcloned into the pCR-II TOPO vector (Invitrogen). The *pkd-2* cDNA (2148 bp) encodes a protein of 715 amino acids. A 1.3 kb *pkd-2* promoter (*Ppkd-2*) encoded by sequence directly upstream of the cDNA start site was amplified from a full length rescuing *pkd-2* genomic PCR product (Barr et al., 2001) and subcloned into *Hin*dIII sites in the Fire Vectors (pPD95.75, pPD95.77 and pPD95.79) to generate the cloning vectors pKK64, pKK49 and pKK50. The plasmid pKK47 (*Ppkd-2*::GFP) is the PCR amplified promoter subcloned into *Hin*dIII and *Bam*H1 sites of pPD95.75.

GFP expression constructs

A P*pkd-2*::PKD-2(cDNA)::GFP construct (pKK52 or PKD-2::GFP) was generated by subcloning the entire *pkd-2* cDNA into pKK49. To target GFP to the ER (endoplasmic reticulum) of male-specific neurons (pYK4, P*pkd-2*::GFP::KDEL), the *pkd-2* promoter was isolated by digestion of pKK47 with *Hin*dIII and *Xho*I, and exchanged with the *myo-3* promoter of P*myo-3*::GFP::KDEL (Labrousse et al., 1999). To generate a rough ER marker in *pkd-2*-expressing neurons, the TRAM cDNA from the Gateway ORFeome library (Reboul et al., 2003) was amplified and inserted into pKK47 between *Sal*I and *Bam*HI sites. To generate P*unc-119*::PKD-2::GFP, PKD-2 cDNA was subcloned into the *Pst*I and *Bam*HI sites in pPD95.77. The 2.4 kb *unc-119* promoter (Maduro and Pilgrim, 1995) flanked by *Pst*I sites was inserted into this construct.

Transgenics

Expression constructs were co-injected with *pha-1(+)* plasmid pBX1 into *pha-1; him-5* (Granato et al., 1994). PKD-2::GFP and P*coelomocyte(cc)::GFP,* (Miyabayashi et al., 1999) were co-injected into *pkd-2(sy606); him-5* (Barr et al., 2001). PKD-2::GFP was integrated into the genome using gamma irradiation to generate two independently integrated lines, *myIs1* and *myIs4*, which were outcrossed six times. *myIs1* LG *IV* or *myIs4* LG*V* was crossed with the appropriate mutant strain.

Microscopy

Confocal images were collected using a 63× (NA 1.4) objective on a BioRad MRC 1024 laser-scanning microscope (Lasersharp2000^{TM} software). Optical sections were collected between 0.4-1.0 μm and projected as *z*-series that were stored as .tif files and manipulated using Adobe PhotoShop. Time-lapse images were obtained with a Nikon Eclipse TE2000 microscope equipped with a 100×, 1.4 NA objective and a Photometrics Cascade 512B with a CCD87 CCD. All the images were collected at exposure time 200 mseconds

per frame, no interval time between frames, with the staged worms anaesthetized with 1 mM levamisole, mounted on agarose pads and maintained at 25°C. Kymographs and movies were created using MetaMorph software. Time lapse movies are available upon request. Epifluorescence analysis was performed on a Zeiss Axioplan2 imaging system and Openlab software (Improvision). Each 12-bit grayscale image focuses on either non-overlapping cilia or cell bodies. For intensity measurements, the ciliary or cell body region was selected to include the whole compartment. The average fluorescence intensity within cilia (F_{cilia}) and cell body ($F_{cell\ body}$) is normalized to the background intensity. All intensity comparisons were performed with images obtained using identical settings (exposure time, gain, offsets) avoiding saturation and with synchronized animals.

Behavioral assays

Male mating assays were performed as described previously (Barr and Sternberg, 1999), except the assays were run for 4 minutes as opposed to 10 minutes. At least 20 animals per genotype were scored per assay. Response efficiency reflects the percentage of the males that responded to the hermaphrodites within 4 minutes. Location of vulva efficiency is calculated by successful vulva location divided by the total number of vulva encounters for each male. Statistical analyses were performed by nonparametric Mann-Whitney tests with two-tailed *P*-value.

RESULTS

GFP-tagged PKD-2 localizes to ER, post-ER puncta and cilia

We generated integrated GFP-tagged PKD-2 (PKD-2::GFP) transgenes to visualize and study how PKD-2 is transported. PKD-2::GFP transgenes fully rescue the male mating defect of *pkd-2(sy606)* null mutants (Fig. 7), indicating that these transgenes are functional. PKD-2::GFP transgene expression patterns are consistent with previous anti-PKD-2 antibody staining (Barr et al., 2001), thereby providing an accurate readout of PKD-2 subcellular localization. *pkd-2* is expressed in a subset of male-specific sensory neurons: four CEM neurons in the head, eight pairs of Ray B neurons (1-5 and 7-9, excluding R6B), and the HOB hook neuron in the tail (Fig. 1A) (Barr et al., 2001; Lints and Emmons, 2002). Each neuron that expresses PKD-2 has an exposed cilium at the distal ending of the dendrite (Sulston et al., 1980; Ward et al., 1975). In these neurons, PKD-2::GFP localizes predominantly to cell bodies and cilia, and is also observed in small dendritic and axonal puncta (Fig. 1B,C). Within the ciliary region, PKD-2::GFP is distributed throughout the cilium, but primarily concentrated at the

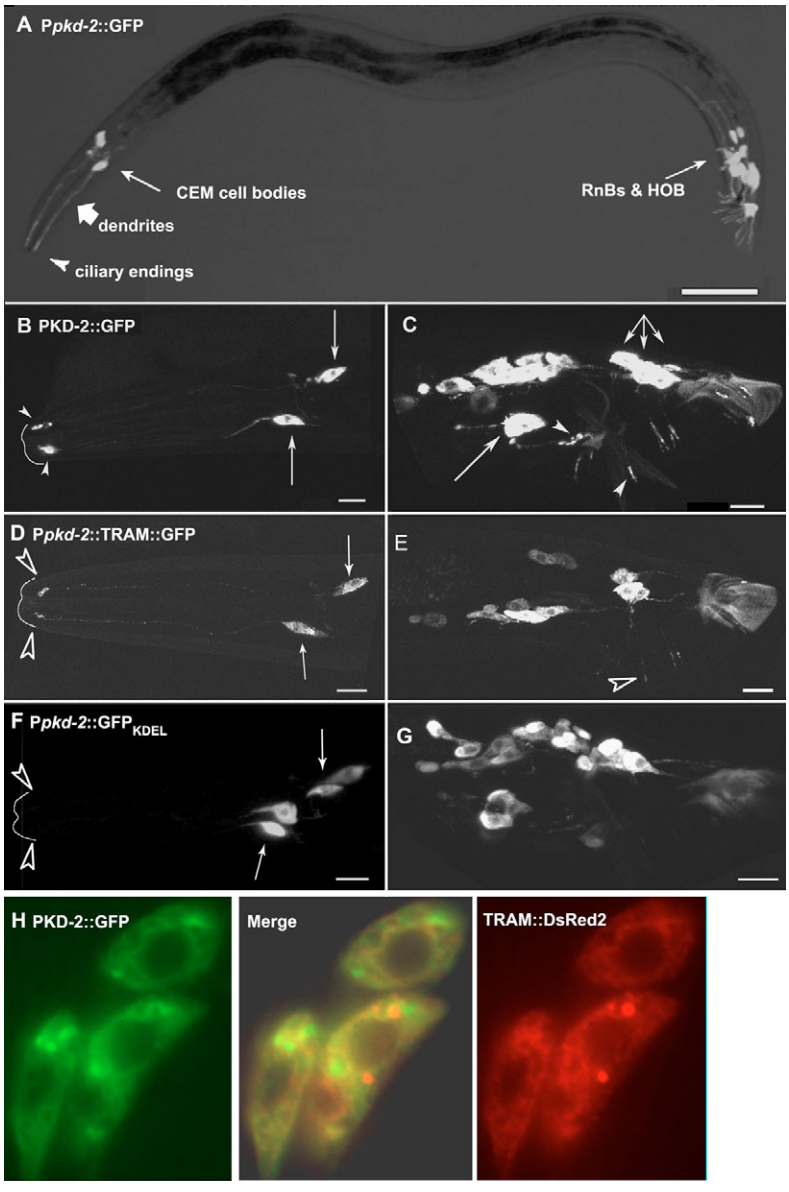

Fig. 1. PKD-2 localizes to cilia and ER in male-specific sensory neurons. (A-G) Images are projected *z*-series obtained by laser-scanning confocal microscopy unless indicated otherwise. (**A**) A lateral view of an adult male expressing P*pkd-2*::GFP (*pkd-2* promoter driving GFP expression). GFP is expressed in four CEMs in the head, 16 ray B neurons, and the HOB neuron in the tail. Scale bar: 100 μm. (**B**,**C**) PKD-2::GFP localizes in the cell bodies (arrows), small dendritic and axonal puncta, and ciliary endings (arrowheads). Scale bars: 10 μm. (B) CEMs, (C) RnB ray (three arrows) and HOB (one arrow) neuronal cell bodies, and ciliary regions (ciliary membrane and base, arrowheads). (**D**,**E**) GFP-tagged TRAM expressed under (P*pkd-2*::TRAM::GFP) localizes in cell bodies (arrows), dendritic puncta and ciliary bases (open arrowheads), but not the cilium proper. Scale bars: 10 μm. (D) CEMs, (E) HOB and RnB neurons. (**F**,**G**) GFP-KDEL ER marker driven by the *pkd-2* promoter shows reticular structure in cell bodies and is excluded from ciliary and dendritic compartment of the cells. Open arrowheads indicate the absence of GFP in cilia. (**H**) Epifluorescence images showing overlapping expression of PKD-2::GFP and P*pkd-2*::TRAM::DsRed2 in RnB cell bodies.

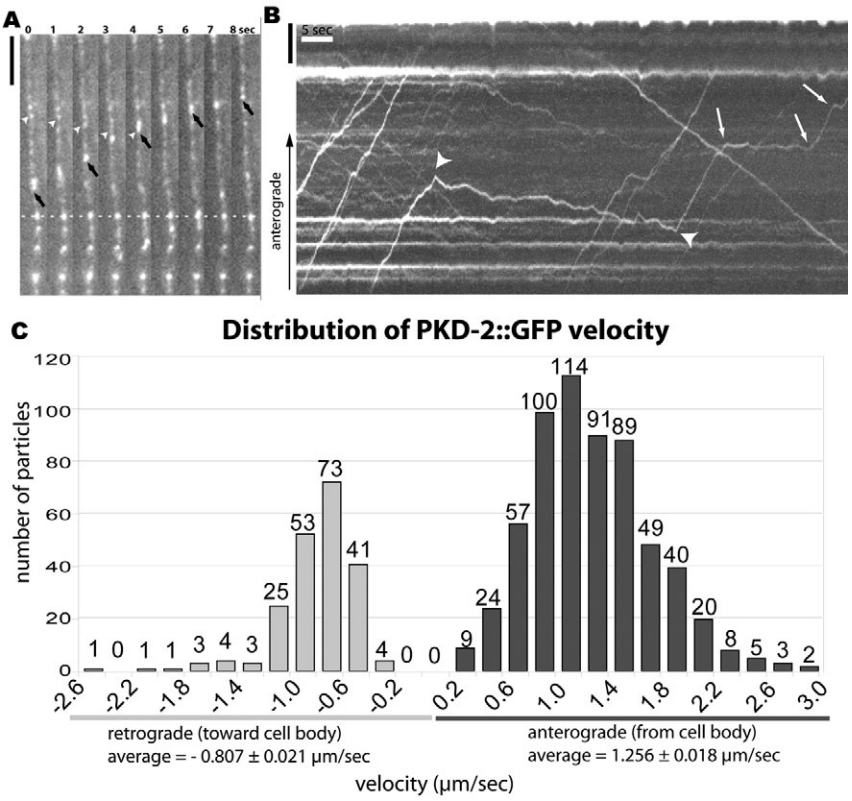

Fig. 2. PKD-2::GFP moves rapidly and bidirectionally in dendrites. (**A**) A montage of PKD-2::GFP particles shows both anterograde (black arrows, from the cell body to cilium) and retrograde (white arrowheads) movement. The broken white line indicates stationary particles. Scale bar: 5 μm. (**B**) A kymograph depicting PKD-2::GFP particle motility in the dendrite. The horizontal and vertical axes represent time and distance, respectively. Vertical scale bar: 5 μm. The left arrowhead illustrates the changes from anterograde to retrograde and the right arrowhead reflects retrograde to anterograde changes. Saltatory movement is also detected (arrows). (**C**) Distribution of PKD-2 particle velocities in dendrites. The particles have distinct velocities for retrograde (light boxes) and anterograde (dark boxes) directions. The velocities are shown as the average ± s.e.m. Time lapse movies are available upon request.

ciliary base, which corresponds to the distal-most dendrite and transition zone regions (refer to cartoon in Table 3 and Fig. 6A) (Qin et al., 2005).

In the cell body, PKD-2::GFP is cytoplasmic and reticular, suggesting that PKD-2 may be present in the endoplasmic reticulum (ER). To visualize ER in PKD-2 neurons, we individually expressed TRAM::GFP, TRAM::DsRed2 and GFP::KDEL driven by a 1.3 kb *pkd-2* promoter. TRAM is a component of ER translocon and localizes to rough ER and also post-ER compartments (Greenfield and High, 1999). Four amino acid KDEL (Lys-Asp-Glu-Leu) is an ER targeting and retention signal (Terasaki et al., 1996). TRAM::GFP and GFP::KDEL were primarily distributed in a tubular membrane structure within the cell body (Fig. 1D-G), but TRAM::GFP was also targeted to dendritic and axonal puncta and the ciliary base, but not the cilium proper (Fig. 1D,E). GFP::KDEL is predominantly located in ER lumen in the cell body (Fig. 1F,G). Double labeling with PKD-2::GFP and TRAM::DsRed2 indicated that the two share an overlapping localization pattern in ER of cell bodies (Fig. 1H). These data suggest that PKD-2 is synthesized in the ER and packaged into vesicles that are transported to the ciliary base and inserted onto the ciliary membrane, as shown for rhodopsin in photoreceptor cells (Deretic and Papermaster, 1991).

PKD-2::GFP particles move rapidly in dendrites

Time-lapse fluorescence microscopy was used to determine if PKD-2::GFP particles move in dendrites of CEM and RnB ray neurons. PKD-2::GFP movement is bidirectional and saltatory; moving particles sometimes stop and then resume movement, occasionally reversing directions (Fig. 2A,B). Depending on directionality, PKD-2::GFP particles move at different rates. Anterograde movement (from cell body to ciliary base) averages 1.260±0.019 μm/sec and retrograde movement (from ciliary base to cell body) averages 0.807±0.021 μm/sec (Fig. 2C and Table 1). The average velocities in CEM and RnB ray neurons are not statistically different (P>0.05), suggesting that the same anterograde and retrograde transport systems are responsible for PKD-2 movement in both cell types.

In dendrites of chemosensory amphid AWB neurons, the ODR-10 G-protein coupled receptor (GPCR) moves at rates similar to PKD-2 (Dwyer et al., 2001). The ODR-10 and PKD-2 ciliary

Table 1. Velocity analysis of PKD-2::GFP particles

	Retrograde	Anterograde
Average velocity (μm/second)	0.807±0.021	1.260±0.019
	CEM: 0.768±0.019 (132)	CEM: 1.239±0.021 (476)
	RnB: 0.872±0.045 (77)	RnB: 1.334±0.042 (135)
Number of particles	209	611
Average video duration (seconds)	4.96±0.31	5.12±0.22
Average movement distance (μm)	3.65±0.21	5.77±0.20
% particles moving (uninterrupted for more than 5 seconds)	30.6	34.4
% particles moving (uninterrupted for more than 5 μm)	16.7	42.7

Average velocities (mean±s.e.m.) reflect the mean rate of each moving particle identified in kymographs. The velocities in CEMs and RnB ray neurons are not significantly different for both the anterograde and retrograde movement. Statistical analysis was performed using nonparametric Mann-Whitney test with two-tailed *P*-value. A total of 38 CEMs and 24 RnB ray neurons were used for the velocity analysis.

Table 2. At least two transport systems act in dendrites.

	Retrograde (μm/second)	Anterograde (μm/second)
PKD-2::GFP	0.807±0.021	1.260±0.019
ODR-10:GFP (Dwyer et al., 2001)	0.71±0.04	1.42±0.09
IFT components (Signor et al., 1999a) (OSM-1::GFP, OSM-6::GFP, KAP-1::GFP)	~1.02	~0.71

receptor proteins are expressed in different sensory neuron cell types, yet exhibit comparable velocities, with faster anterograde (~1.3-1.4 μm/second) than retrograde (~0.7-0.8 μm/second) movement (Table 2). The ciliary IFT machinery must also travel through dendrites to reach cilia. The rate of PKD-2 and ODR-10 dendritic movement is significantly different than published dendritic velocities of IFT components (Table 2) (Signor et al., 1999a), suggesting that the dendritic transport of ciliary receptors and the IFT machinery involves different motors. These data support the model that a common transport machinery operates in dendrites to move sensory receptors to and from ciliary bases.

UNC-101 is required for the somatodendritic targeting of PKD-2

The AP-1 μ1 clathrin adaptor UNC-101 is required for restricting ODR-10 and OSM-9 to dendrites (Dwyer et al., 2001). To determine whether PKD-2 also employs UNC-101, we examined PKD-2 localization in *unc-101* mutants. In *unc-101(m1)* and *unc-101(sy108)* males, PKD-2::GFP is uniformly distributed throughout the entire neuron, including the axon, dendrite, cell body and cilium (Fig. 3D-F). There is no obvious difference in ER localization of PKD-2 in the *unc-101* background. We could not detect individual PKD-2::GFP particle movement in *unc-101* dendrites because the fluorescent protein is distributed evenly throughout the neuronal processes. These data indicate that UNC-101 acts at the somatodendritic sorting step, which is required for directing PKD-2 to dendrites and cilia.

The μ1 subunit of AP-1 recognizes cargo proteins via tyrosine-based [Yxxϕ, ϕ: a bulky hydrophobic amino acid] or dileucine [D/ExxxLL/I or DxxLL] sorting signals in cytoplasmic domains of membrane proteins (Bonifacino and Traub, 2003). The N- and C-termini of PKD-2 contain one and four putative UNC-101 recognition motifs, respectively. If UNC-101 directly interacts with PKD-2, then mutation or deletion of these recognition signals should affect PKD-2 localization. Neither site-directed mutagenesis nor deletion of the N and C termini affects PKD-2 somatodendritic or ciliary localization (Hu et al., 2006) (K.M.K., Y-K.B., J.H. and M.M.B., unpublished). These results indicate that the cytoplasmic domains of PKD-2 are not essential for somatodendritic or ciliary targeting in vivo.

We find that other adaptor protein (AP) complex components are not essential for regulating the subcellular localization of PKD-2. AP complexes mediate clathrin-coated vesicle (CCV) formation at

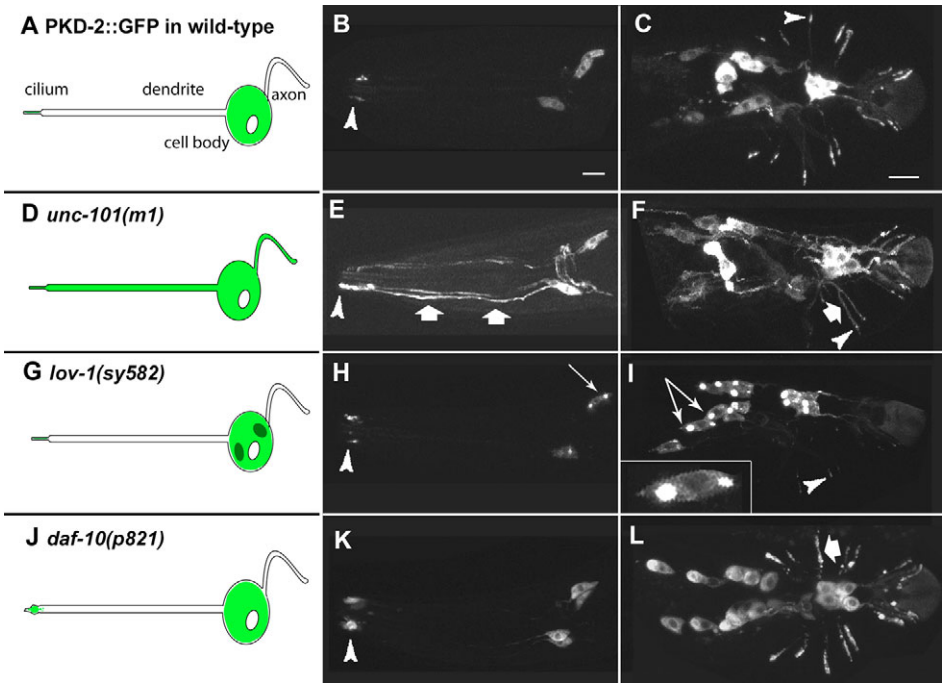

Fig. 3. PKD-2::GFP localization is altered in *unc-101*, *lov-1* and IFT mutants. (A,D,G,J) Cartoons of a sensory neuron expressing PKD-2::GFP (shown in green) for each genotype. (B,E,H,K) CEMs, (C,F,I,L) RnBs and HOB neurons. (**A-C**) Wild-type localization of PKD-2::GFP. PKD-2 in ciliary endings (ciliary membrane and ciliary base, arrowheads) in CEMs and RnBs. (**D-F**) In *unc-101(m1)* mutants, PKD-2::GFP is uniformly distributed throughout neurons, including axons, cell bodies, dendrites (thick arrows) and cilia (arrowhead). (**G-I**) In *lov-1(sy582)* mutants, PKD-2::GFP aggregates within the cell bodies (arrows) and is expressed in a lower level in ray cilia (arrowhead in 3I). The boxed inset in I shows a closer view of a ray cell body containing PKD-2::GFP aggregates. (**J-L**) In *daf-10(p821)* mutants, PKD-2::GFP accumulates in the ciliary base (arrowheads). In the RnBs, PKD-2::GFP also mislocalizes to dendrites (thick arrow). This mutant phenotype is consistent in other IFT single and double mutant backgrounds. Scale bars: 10 μm.

various membrane structures in cells. Of these, AP-1 contains four subunits (γ, β1, μ1 and σ1) and localizes in the membrane of *trans*-Golgi network (TGN) and endosomes. *apm-1* encodes *C. elegans* μ1-II subunit of AP-1 complex (Shim et al., 2000). In contrast to *apm-1* RNAi L1 larval arrest (Shim et al., 2000), the of *apm-1(cxP9732)* reduction-of-function allele is viable (Martin et al., 2002). In *apm-1(cxP9732)* mutants, PKD-2::GFP localizes properly in cilia and cell bodies, suggesting an AP-1 complex with APM-1 as the medium subunit is not involved in PKD-2 targeting. Alternatively, residual *apm-1* function may be sufficient to ensure proper PKD-2 localization.

AP-2 and AP-3 are involved in endocytosis at plasma membrane and lysosomal-related organelle transport, respectively (Bonifacino and Traub, 2003). Mutations in the AP-2 and AP-3 complex [*dpy-23(e840), apt-6 (ok429)* and *apt-7(tm920)*] do not obviously affect PKD-2 dendritic or ciliary localization. UNC-11, the *C. elegans* homologue of a clathrin adaptor AP180, acts at pre- and postsynaptic regions to regulate clathrin-mediated endocytosis (Burbea et al., 2002; Nonet et al., 1999). We find that *unc-11(e47)* mutation does not alter PKD-2 localization to the dendrite or cilium. A GTPase dynamin is a central player in internalization of membrane proteins via clathrin-mediated endocytosis along with AP-2 complex (Brodsky et al., 2001). PKD-2::GFP dendritic and ciliary localization was not obviously altered in *dyn-1(ky51)* mutants. We conclude that UNC-101 acts at a somatodendritic sorting step to restrict PKD-2, along with other ciliary receptors, to the dendritic compartment.

PKD-2::GFP in the following mutants is not different from wild type: β-arrestin single mutant *arr-1(ok401)*; kinesin and kinesin-related single mutants *unc-116 (e2310)*, *unc-16 (ju146, e109)*, *klp-10 (ok704, tm375)*, *unc-104 (e1265)* and *klp-16 (ok1505)*; dynein single mutants *dhc-1(or195ts)* and *dnc-1(or404ts)*; axonal outgrowth single mutants *unc-33(e204)* and *unc-44(e362)*; and lipid raft single mutants *cav-1(ok274)* and *cav-2(tm394)*.

PKD-2 requires LOV-1 for efficient somatodendritic and ciliary targeting

Ion channels often require functional partner proteins for appropriate folding and targeting. To test whether PKD-2 requires its functional partner LOV-1 for ciliary targeting, we examined the localization of PKD-2::GFP in the null mutant *lov-1(sy582)*. To quantify any changes in PKD-2::GFP abundance, we measured fluorescence intensity in cilia (F_{cilia}) and the cilium to cell body ratio ($F_{cilia}/F_{cell\ body}$) (Fig. 4). The F_{cilia} reflects the absolute abundance of PKD-2::GFP in cilia and the $F_{cilia}/F_{cell\ body}$ ratio measures the relative PKD-2::GFP level in the cilium to the cell body. In CEMs, PKD-2::GFP ciliary abundance in a *lov-1* background is not significantly different from wild type (Fig. 4A). In rays, however, PKD-2 is often absent from RnB cilia (Fig. 4C). Moreover, the fluorescence intensity in those ray cilia with detectable PKD-2::GFP is largely reduced compared with wild type (Fig. 4D,E). We conclude that LOV-1 plays a tissue-specific role and is required for efficient somatodendritic and ciliary targeting of PKD-2 in ray but not CEM neurons.

In both the CEMs and RnBs of a *lov-1* mutant, PKD-2::GFP forms one or two large aggregates in cell bodies (Fig. 3G-I). This aggregation phenotype is more severe in RnBs than CEMs, which may account for frequent loss of PKD-2 in ray cilia (Fig. 4C). PKD-2 may be retained within the ER in the absence of LOV-1. However, aggregate appearance does not resemble the normal ER structure

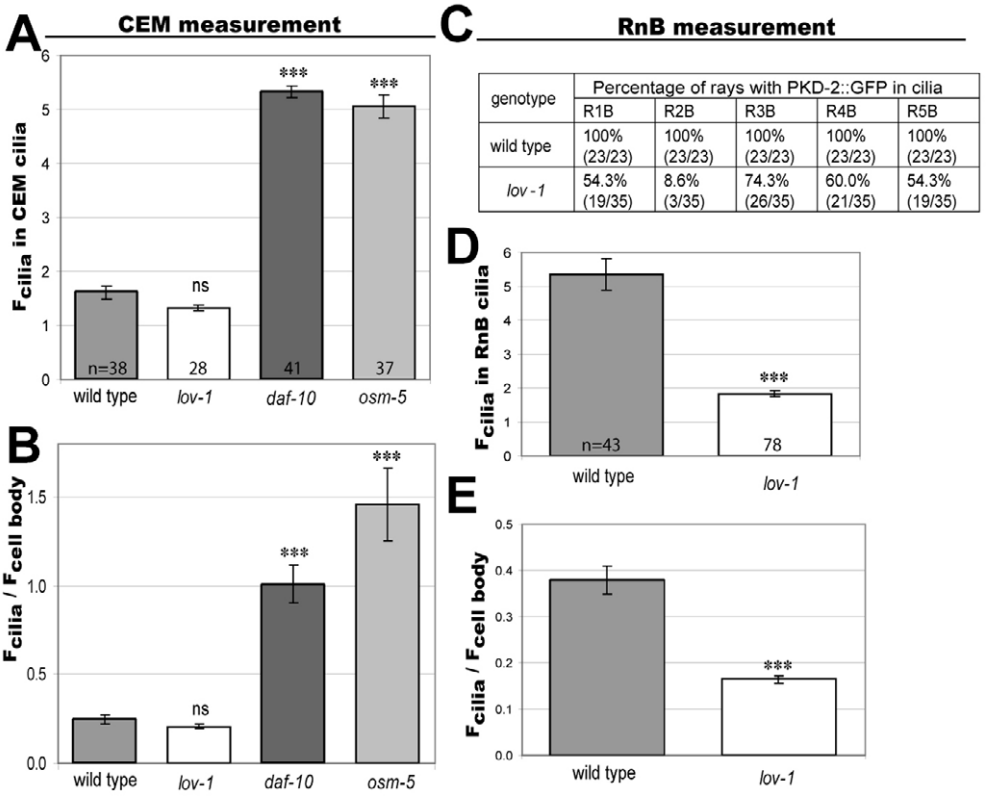

Fig. 4. PKD-2::GFP abundance in cilia is altered in *lov-1* and IFT mutants. (**A**,**B**) Fluorescence intensity in CEM cilia (F_{cilia}) shows that PKD-2::GFP accumulates in IFT mutants. (A) F_{cilia} of PKD-2::GFP in CEMs in wild-type, *lov-1*, *daf-10* and *osm-5* backgrounds. F_{cilia} in the IFT mutants (*daf-10* and *osm-5*) is approximately three times greater than in wild type. (B) Ratio (F_{cilia} /$F_{cell\ body}$) shows that PKD-2::GFP abundance in CEM cilia is increased in comparison with the cell bodies in IFT mutants (*daf-10* and *osm-5*). (**C-E**) Fluorescence intensity measurement in RnB ray cilia of wild type and *lov-1* mutants reveals reduced ciliary localization in *lov-1* background. (C) PKD-2::GFP localization in RnB ray cilia is often below detectable levels in *lov-1* mutants. R1B to R5B are selected because they are easily distinguished from other rays. The percentage reflects the number of rays exhibiting detectable ciliary localization divided by total number of ray pairs scored. Those cilia with detectable GFP were used for ciliary measurement in D and E. (D) F_{cilia} in RnB cilia showed that PKD-2::GFP levels in *lov-1* mutants are significantly reduced. (E) F_{cilia} /$F_{cell\ body}$ ratio in rays reveals decreased PKD-2::GFP ciliary abundance in *lov-1* mutants. Error bars indicate s.e.m. Non-parametric Mann-Whitney tests with two-tailed *P*-value were performed between wild type and each genotype. ns, not significant ($P>0.05$); ***$P<0.001$; n, number of cilia measured.

(compare with Fig. 1D-H). The aggregates may represent an altered ER structure caused by misfolded PKD-2, or may result from the targeting of PKD-2 to an unidentified subcellular compartment. We conclude that LOV-1 plays a crucial role in PKD-2 localization within neuronal cell bodies.

We next examined PKD-2::GFP dendritic motility in the *lov-1* mutant. PKD-2::GFP particles exhibit similar bidirectional movement as wild type in the *lov-1* dendrite. These data suggest that *lov-1* is not required for PKD-2::GFP dendritic motility.

For proper somatodendritic sorting, PKD-2 requires UNC-101 and LOV-1. To determine the order of action, we examined PKD-2::GFP localization in the *unc-101(m1); lov-1(sy582)* double mutant. In the double mutant, as in *unc-101* alone, PKD-2::GFP is distributed throughout the neuron and does not aggregate in cell bodies (data not shown). These data suggest that *unc-101* acts at the somatodendritic sorting step before *lov-1*.

Additional cell-type specific factors are necessary for PKD-2 somatodendritic targeting

pkd-2 and *lov-1* are specifically expressed in a subset of male sensory neurons and not observed in other ciliated cell types of males or hermaphrodites. To determine whether PKD-2 subcellular localization requires cell-type specific factors or simply uses a general transport machinery, we ectopically expressed PKD-2::GFP using the pan-neuronal *unc-119* promoter (Maduro and Pilgrim, 1995). P*unc-119*::PKD-2::GFP is localized in the cell bodies of amphid and outer labial quadrant (OLQ) sensilla of the hermaphrodite head, but never observed in amphid or OLQ cilia (Fig. 5A,I). In the tail, P*unc-119*::PKD-2::GFP localizes to the cell bodies of the ciliated phasmid neurons but not their cilia (Fig. 5B). Another example comes from the R6B neurons, which do not normally express *pkd-2* or *lov-1*. P*unc-119*::PKD-2::GFP is absent from R6B cilia; however, PKD-2::GFP is localized properly in R1-

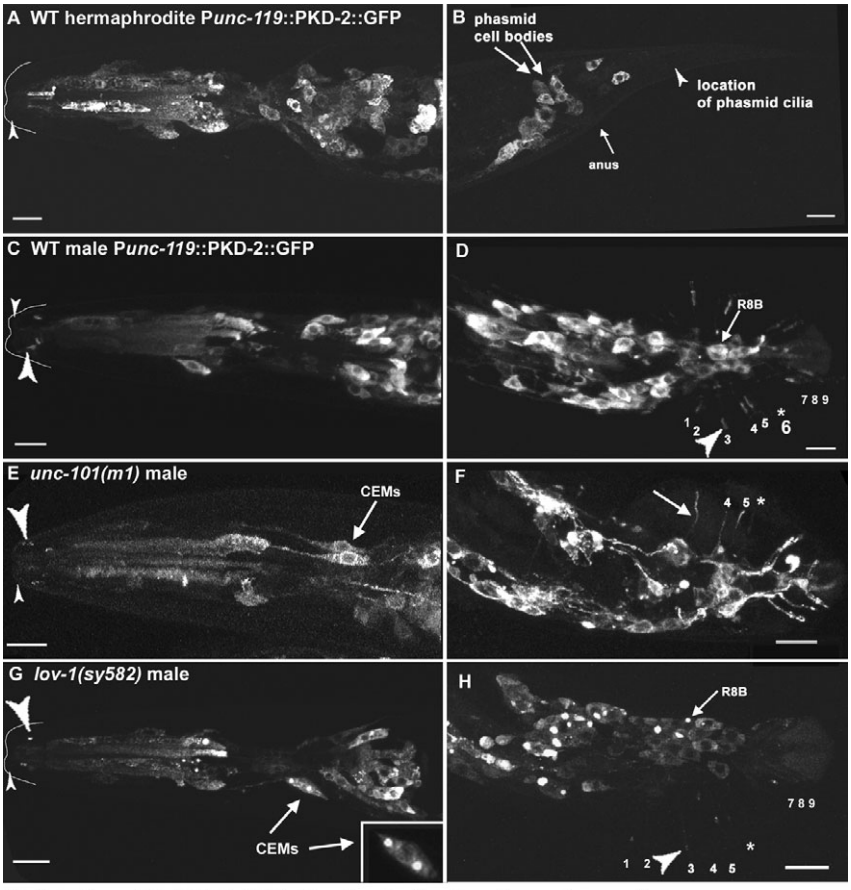

I Table. P*unc-119*::PKD-2::GFP ciliary localization in native and non-native neurons

	native neurons			non-native neurons		
cell type	R3B	R4B	R5B	R6B	phasmid	OLQ
percentage of ciliary localization	92.6% (100/108)	93.5% (101/108)	97.2% (105/108)	3.7% (4/108)	0% (0/112)	0% (0/112)

Fig. 5. Ectopic PKD-2 expression (P*unc-119*::PKD-2::GFP) reveals cell-type specific factors required for PKD-2 localization. (**A**,**B**) A wild-type hermaphrodite expressing P*unc-119*::PKD-2::GFP. (A) PKD-2::GFP localizes to neuronal cell bodies in the head, but GFP is excluded from ciliary endings. Small arrowheads indicate the anatomical location of OLQ (outer labial quadrant) cilia in the left panels. PKD-2::GFP is absent from cilia in the head sensillae of the adult hermaphrodite. (B) In the hermaphrodite tail, PKD-2::GFP is retained in cell bodies of many neurons including the ciliated phasmid sensory neurons. Phasmid cell bodies were identified by their location (arrows); small arrowhead indicates approximate anatomical location of phasmid cilia. PKD-2::GFP is absent from cilia in the phasmids of the adult hermaphrodite. (**C**,**D**) A wild-type male expressing PKD-2::GFP in every neuron. (C) In the head, PKD-2::GFP is localized to the ciliary endings of CEMs (large arrowheads in the left panels). (D) In the male tail, PKD-2::GFP is detected in ciliated endings (large arrowhead, R3B cilium) of all B-type ray neurons, except R6B (asterisk), which does not normally express the polycystins. (**E**,**F**) P*unc-119*::PKD-2::GFP expression in the *unc-101(m1)* mutant. Arrows indicate PKD-2::GFP dendritic expression in polycystin-expressing neurons. (E) In the head, PKD-2::GFP is distributed throughout male-specific CEM neurons. In all other neurons, PKD-2::GFP remains in cell bodies. (F) In the tail, PKD-2::GFP is uniformly distributed only in all B-type ray neurons (arrow) except R6B (asterisks). *unc-101* males are Mab (male abnormal) and often fail to develop all ray process. (**G**) In the *lov-1* mutant, PKD-2::GFP aggregates in CEM cell bodies (arrows) but not in other neurons, and PKD-2::GFP is detectable in CEM cilia (large arrowheads), which are identified by location and cell body morphology. The inset shows one CEM cell body with PKD-2::GFP aggregates (compare with the Fig. 3I inset). A subset of *z*-series confocal sections is projected to generate the inset. (**H**) PKD-2::GFP in *lov-1* RnB ray neurons forms aggregates in cell bodies (arrow), and the level of ciliary staining is reduced. Large arrowhead points at R3B cilia with reduced PKD-2 expression. Scale bars: 10 μm. The anterior outlines of the worm are drawn by hand according to the transmission images. (**I**) The percentage of ciliary localization of P*unc-119*::PKD-2::GFP in non-native and native cells. The reason that a small fraction (3-7%) of native cells do not localize PKD-2::GFP in native cilia may be due to mosaicism of the extrachromosomal array. When PKD-2::GFP is detected in R6B cilia, PKD-2::GFP staining is reduced and mislocalized to the distal dendrite. In the hermaphrodite, there is no detectable ciliary PKD-2::GFP expression in the head. Specifically, OLQ cilia were scored because of their distinct shape and location. One-hundred and eight pairs of RnBs were scored. For hermaphrodites (OLQs and phasmids), a total of 112 animals were scored. There are four OLQ and phasmid neurons in each animal. WT, wild type

5B and R7-9B cilia (Fig. 5D). Similar to endogenous PKD-2, P*unc-119*::PKD-2::GFP localizes to cilia in greater than 92% of R3-5Bs. By contrast, P*unc-119*::PKD-2::GFP is found in cilia in less than 4% of R6B neurons (Fig. 5I). In the small number of animals with PKD-2::GFP in R6B cilia, PKD-2::GFP mislocalizes to distal dendrites, suggesting improper targeting. Alternatively, PKD-2 expression in R6B may an artifact of transgene overexpression. Hence, P*unc-119*::PKD-2::GFP localizes to cilia in only endogenous polycystin-expressing neurons and the PKD-2 somatodendritic sorting step requires cell-type specific factors.

To test the order of action between the cell-type specific factors and UNC-101, we examined P*unc-119*::PKD-2::GFP in the *unc-101* mutant. In *unc-101* animals, P*unc-119*::PKD-2::GFP is uniformly distributed throughout only native polycystin-expressing neurons (Fig. 5E,F). In other cell types in the male and all neurons in the hermaphrodite, P*unc-119*::PKD-2::GFP is retained in cell bodies (Fig. 5E,F; data not shown). This data suggests mislocalization of PKD-2 to the entire neuron in *unc-101* requires cell-type specific factors. We propose that cell-type specific factors associate with the UNC-101/AP-1 complex to restrict PKD-2 to the somatodendritic compartment.

One candidate cell-type specific factor is LOV-1, the partner of PKD-2. To determine whether LOV-1 is the sole cell-type specific factor, P*unc-119*::PKD-2::GFP was examined in the *lov-1* mutant. In the *lov-1* mutant, P*unc-119*::PKD-2::GFP fluorescence intensity in ray cilia is reduced compared with wild type, and RnB ciliary localization was often lost (Fig. 5H). In *lov-1* mutants, P*unc-119*::PKD-2::GFP aggregates are only observed in RnB, HOB and CEM cell bodies (Fig. 5G,H). Hence, the absence of LOV-1 is not sufficient for PKD-2 aggregation in non-native neurons and additional cell-type specific factors act before *lov-1* and *unc-101* in the PKD-2 somatodendritic sorting step.

Intraflagellar transport regulates PKD-2 ciliary abundance

PKD-2 accumulates at the ciliary bases of *osm-5/IFT88/Polaris* mutants (Qin et al., 2001). However, PKD-2 motility is not detected in wild-type cilia (Qin et al., 2005). To further explore the relationship between IFT and PKD-2 ciliary protein abundance, we characterized PKD-2::GFP distribution and dendritic motility in various IFT mutants, including complex A *daf-10(p821)* (Qin et al., 2001; Bell et al., 2006); complex B *osm-5(m184), osm-5(mn397)* and *che-13(e1805)* (Haycraft et al., 2003; Qin et al., 2001); and complex A/complex B double *daf-10; osm-5* and *daf-10; che-13* mutants. We also examined kinesin and dynein single mutants *osm-3(p802)* (Shakir et al., 1993), *klp-11(tm324)*, *kap-1(ok676)* (Snow et al., 2004) and *che-3(e1124)* (Signor et al., 1999a; Wicks et al., 2000), and *osm-3; kap-1* and *klp-11; kap-1* double mutants.

In wild type, PKD-2 is enriched at the ciliary base and observed at lower and variable levels within the ciliary membrane (Fig. 6A). In a stark contrast to wild type, all IFT mutants examined abnormally accumulate PKD-2::GFP in the ciliary base and in the cilium for those mutants with ciliary axonemes (Fig. 3J-L; Fig. 4A,B; Fig. 6B-E). In RnB neurons of IFT mutants, PKD-2::GFP accumulation extends into the distal dendrites (Fig. 3L, thick arrow). In the CEMs, PKD-2::GFP levels in cilia are increased approximately threefold in both *daf-10* complex A IFT122 and *osm-5* complex B IFT88 mutants when compared with wild type (Fig. 4A,B). In *osm-5* mutants, the ratio ($F_{cilia}/F_{cell\ body}$) is greater than *daf-10* because the $F_{cell\ body}$ is reduced in *osm-5* animals (Fig. 4B). These results suggest that, in the absence of IFT, PKD-2 is not properly removed from the ciliary compartment or the dendritic movement from cilia to cell body is compromised. Alternatively, PKD-2::GFP accumulation may be an indirect effect of abnormal cilium structure.

To discriminate between these possibilities, we started by examining CEM ciliary structure by labeling ciliary microtubules with DsRed2 tagged-β-tubulin (P*pkd-2*::TBB-4::DsRed2, Fig. 6). *tbb-4* is expressed in ciliated neurons (Portman and Emmons, 2004), including ray neurons and CEMs, the latter are shown in Fig. 6A-E. In wild type, the CEM ciliary axonemes are symmetrically arranged, with cilia bending outward with respect to the buccal cavity (Fig. 6A). PKD-2::GFP is enriched at the ciliary base and along the ciliary membrane (Qin et al., 2005). In most IFT mutants, CEM cilia defects are similar to those described in amphid cilia (Perkins et al., 1986). In *osm-3* and *osm-5* mutants, CEM cilia are stunted and often possess abnormal projections, and PKD-2 accumulates in ciliary bases and along the shortened cilia at variable levels (Fig. 6B,C). *che-3* cilia are longer than wild type, and abnormal PKD-2 accumulation is observed at the ciliary base and along the ciliary membrane (compare Fig. 6D with wild type in Fig. 6A). PKD-2::GFP similarly accumulates in *klp-11* and *kap-1*, the two kinesin II mutants (Fig. 6E, only *klp-11* is shown). We conclude that in IFT mutants, PKD-2 is capable of entering the ciliary membrane, whether stunted or bent (see below), and accumulates both in the ciliary base and membrane. These data indicate that IFT is not essential for PKD-2 targeting to the ciliary base, but may play a role in regulating PKD-2 levels within the ciliary compartment. However, we cannot formally rule out indirect effects caused by abnormal structure.

The *C. elegans* BBS proteins BBS-7 and BBS-8 stabilize IFT particle complexes and are partially required for the formation of amphid distal cilia (Ansley et al., 2003; Blacque et al., 2004; Ou et al., 2005). In *bbs-7(osm-12)* mutants, PKD-2 subcellular localization and male mating is indistinguishable from wild type (Barr and Sternberg, 1999) (data not shown). These data indicate that BBS-7 function is not required for regulating PKD-2 ciliary localization or function.

We next determined whether IFT plays a role in PKD-2 dendritic transport. In addition to a role in cilia, kinesin 2 has been implicated in other microtubule based transport systems (Brown et al., 2005; Miller et al., 2005). IFT components such as OSM-6, OSM-5, OSM-3 and KAP-1 are also detected in dendrites of sensory neurons including male-specific neurons (Collet et al., 1998; Qin et al., 2001; Signor et al., 1999b) (Fig. 6F, arrow). To determine whether any IFT motors or polypeptides are essential for the dendritic transport of PKD-2, we examined PKD-2::GFP dendritic motility in IFT mutants. In all IFT mutants examined, PKD-2::GFP dendritic motility is still observed, confirming the primary role of IFT in the ciliary compartment. Combined, these data suggest that IFT may regulate PKD-2 ciliary abundance via removal from the cilium.

Kinesin II modulates CEM ciliary morphology and male sensory behaviors

Ciliary accumulation of sensory receptors such as PKD-2 may result in profound physiological consequences. Many IFT mutants with general ciliogenesis defects exhibit male mating defects (Barr and Sternberg, 1999; Hodgkin, 1983; Perkins et al., 1986; Qin et al., 2001). In the IFT mutants examined previously, it was unclear whether PKD-2 accumulation in male-specific cilia or general sensory defects account for mating behavioral abnormalities.

Anterograde movement of IFT in *C. elegans* amphid cilia requires two types of Kinesin II motors: homodimeric OSM-3 and heterotrimeric kinesin II (KLP-11/KAP-1/KLP-20) (Snow et al.,

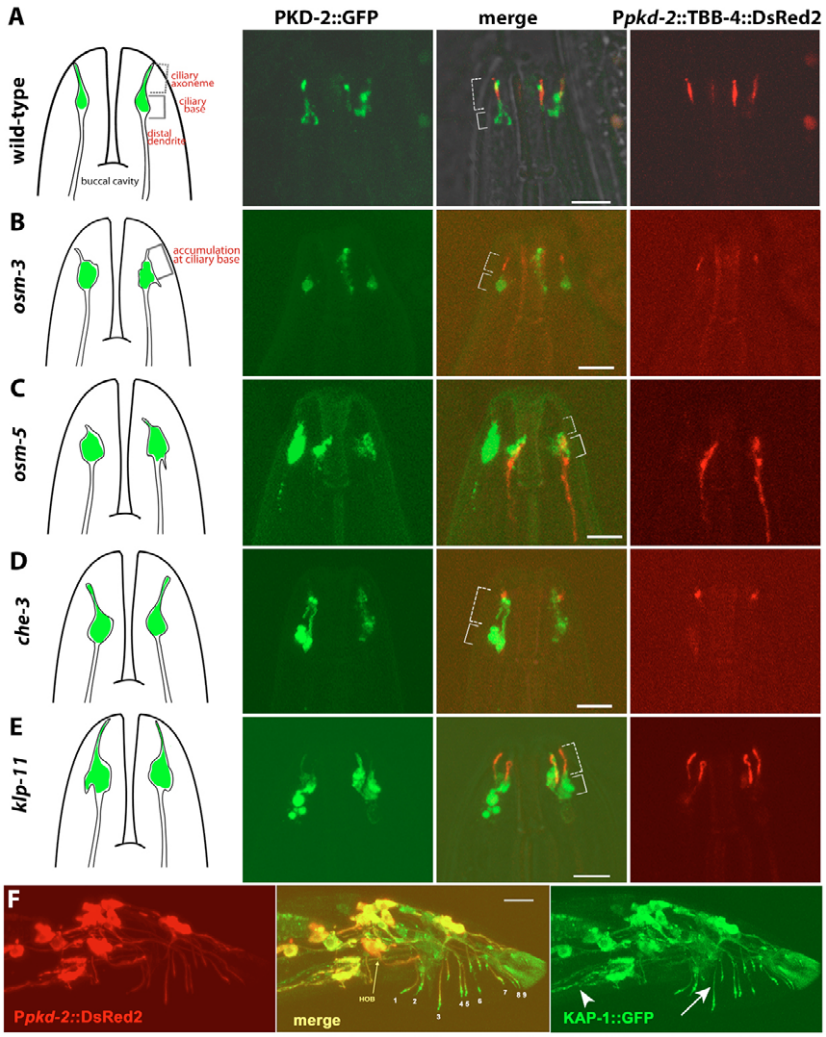

Fig. 6. PKD-2::GFP CEM ciliary distribution in wild type and IFT mutants. The first column depicts a cartoon showing two out of four CEM cilia in the male nose. Column 2 shows PKD-2::GFP ciliary distribution patterns. Column 4 shows P*pkd-2*::TBB-4::DsRed2 labeling CEM ciliary axonemes of wild type and IFT mutants. Column 3 is the merged image of Columns 2 and 4. Scare bars: 5 μm. (**A**) In wild type, PKD-2::GFP is enriched in the ciliary base (transition zone and distal-most dendrite, bracket) and along the ciliary membrane (dashed bracket). (**B-E**) PKD-2::GFP accumulates in the ciliary bases (bracket) and abnormal cilia (dashed bracket) of IFT mutants (B,C) In *osm-3* and *osm-5* mutants, PKD-2::GFP accumulates at the bases of stunted cilia. (D) In the *che-3* cytoplasmic dynein mutant, cilia form and PKD-2 accumulates at the ciliary bases and along the ciliary membrane. (E) In the *klp-11* kinesin II mutant (and *kap-1*, not shown), CEM cilia morphology is abnormal and PKD-2 accumulates at ciliary bases and along the ciliary membrane. (**F**) Kinesin II is expressed in polycystin-expressing neurons. The polycystin-expressing neurons are labeled with a *pkd-2* promoter driven DsRed2 (left panel). KAP-1::GFP (right panel) is enriched in the ciliary compartment, but also found in dendrites (arrow) and axons (arrowhead). HOB, hook B neuron. (A) Reproduced, with permission, from Qin et al. (Qin et al., 2005).

2004). *osm-3(p802)* and *kap-1(ok676)* are probably null, and *klp-11(tm324)* may be a hypomorph (Snow et al., 2004). Similar to *osm-3* and other IFT mutants, PKD-2::GFP accumulates at the ciliary base and in the cilium in *klp-11*, *kap-1* and *klp-11; kap-1* single and double mutants (Fig. 6E, data not shown). However, the phenotype in *kap-1* and *klp-11* is distinct from other IFT mutants in two respects. First, *klp-11* and *kap-1* mutants develop full-length CEM cilia and amphid cilia but exhibit AWC-specific sensory defects (Evans et al., 2006). Second, CEM cilia adopt an inward trajectory, rather than an outward bend (Fig. 6E). This is the first report of morphology changes in cilia of kinesin II mutants.

To clarify the relationship between PKD-2 localization and sensory function, we performed male mating behavior assays in kinesin motor mutants (Fig. 7). *osm-3(p802)* animals have severely reduced response and vulva location efficiencies (Fig. 7). The Lov (location of vulva) defect of *osm-3(p802)* mutants is comparable with other IFT mutants with general ciliogenesis defects (Barr and

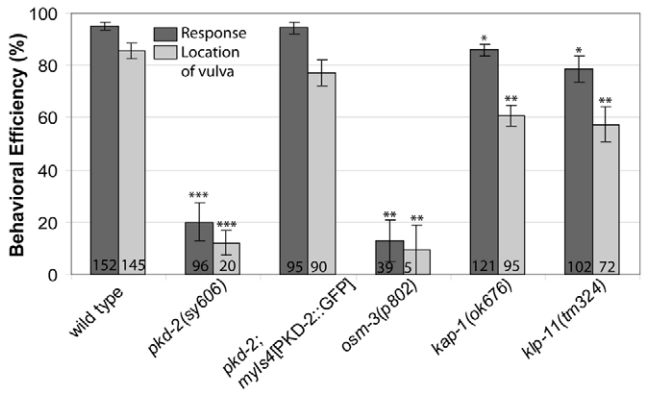

Fig. 7. Male mating behavior is abnormal in IFT mutants. Response and location of vulva efficiency is scored for each genotype. Two independent integrated PKD-2::GFP transgenic lines (*myIs1* and *myIs4*) rescue Response and Lov defects of the *pkd-2* mutant (only *myIs4* is shown). Three IFT kinesin mutants (*osm-3, kap-1, klp-11*) exhibit Response and Lov defects. Non-null *osm-3(e1806)* exhibits wild-type male mating behavior (Barr and Sternberg, 1999). Error bars indicate s.e.m. between multiple assays, and each assay consisted of at least 20 animals. An asterisk marks wherever the data are significantly different from wild type (*P<0.05, **P<0.01, ***P<0.001). n, number of males examined.

Sternberg, 1999). However, *kap-1* and *klp-11* single mutants exhibit slight but significant reduction of response and vulva location efficiencies (Fig. 7). These data indicate that PKD-2::GFP ciliary accumulation in *klp-11* and *kap-1* mutants compromises PKD-2 sensory function. The subtle ciliogenesis defects of kinesin II mutants strongly suggest a causal link between PKD-2 mediated sensation and the regulation of polycystin ciliary abundance by IFT. Alternative but not mutually exclusive explanations are that kinesin II is involved in transporting downstream signaling molecules or that subtle morphological changes in kinesin II mutant cilia account for behavioral defects.

DISCUSSION

Ciliary localization of polycystins is conserved from worm to human. In *C. elegans* sensory neurons, cilia are located at the distal-most somatodendritic compartment, while in mammalian kidney epithelial cells, primary cilia project off the apical surface. How are TRPP1 and TRPP2 targeted to cilia in these two different systems? Our data suggest that the somatodendritic and ciliary sorting steps control the subcellular localization of PKD-2 in *C. elegans* sensory neurons, and that each step involves both general and cell-type specific factors (Table 3). Dynamically moving PKD-2::GFP particles are detected in dendrites of male specific sensory neurons. The ciliary proteins PKD-2 and ODR-10 employ the same dendritic transport system (Dwyer et al., 2001).

UNC-101, the μ1 subunit of AP-1, is required for directing PKD-2, ODR-10 and OSM-9 to dendrites of sensory neurons (Dwyer et al., 2001). In the absence of UNC-101 and in its native environment, PKD-2::GFP is distributed throughout the neuron (Fig. 3D-F, Table 3). Hence, UNC-101 appears to play a general role in directing ciliary membrane receptors to the dendritic compartment in diverse cell types. Somatodendritic transport in neurons shares common features with the basolateral transport in epithelial cells (Bredt, 1998). UNC-101 may be analogous to the μ1B subunit of the epithelial specific AP-1B complex, which mediates basolateral sorting. Is ciliary sorting in mammalian epithelial cells and in *C. elegans* sensory neuron comparable? Is apical sorting prerequisite for ciliary sorting in epithelia cells (or is basolateral sorting a prerequisite for ciliary sorting in sensory neurons)? In kidney epithelia, polycystins are found in the basolateral compartment in addition to cilia, yet have not been described on the apical surface (Pazour et al., 2002; Yoder et al., 2002), suggesting ciliary and apical sorting may involve distinct mechanisms.

Mammalian TRPP2 forms a complex with the γ subunit of AP-1 and with PACS-1 (phosphofurin acidic cluster sorting protein) and this association regulates TRPP2 ER versus plasma membrane localization (Kottgen et al., 2005). The mechanisms regulating mammalian TRPP2 ciliary localization were not explored in this study. There is a PACS-1-like protein (T18H9.7) encoded in the *C. elegans* genome. However, unlike the mammalian counterpart, *C. elegans* TRPP2/PKD-2 does not contain the acidic cluster to which PACS-1 binds, suggesting that PACS-1 may not play a role in PKD-2 localization in *C. elegans* sensory neurons.

In addition to *unc-101*, PKD-2 requires cell-type specific factors at the somatodendritic sorting step. When expressed pan-neuronally, PKD-2::GFP localizes to dendrites and cilia of only native neurons (Fig. 5). In non-native neurons, PKD-2 remains in the cell body (Fig. 5, Table 3). Similarly, the ODR-10 olfactory receptor also requires cell-type specific factors ODR-4 and ODR-8 for ciliary localization (Dwyer et al., 1998). Cell type-specific factors act to functionally specify a cilium and are predicted to possess a restricted expression pattern. Four novel *cwp* (co-expressed with polycystins) genes possess an expression pattern identical to *pkd-2* and *lov-1* (Portman and Emmons, 2004). Future investigation on the cellular and molecular roles of the *cwp* genes is warranted.

LOV-1/TRPP1, the functional partner of PKD-2/TRPP2, is an obvious example of a cell-type specific factor. In *lov-1* mutants, PKD-2::GFP aggregates within cell bodies of both CEM and ray neurons and localizes to cilia at significantly reduced levels only in ray neurons. We propose that *lov-1* may act at both somatodendritic and ciliary steps. At the somatodendritic sorting step, *lov-1* may act after *unc-101* to stabilize PKD-2 within the cell body. At the ciliary sorting step, *lov-1* may stabilize PKD-2 in cilia in a cell-type specific way. In mammalian systems, the requirement of TRPP1 for TRPP2 ciliary targeting depends on the cell culture type (Geng et al., 2006; Nauli et al., 2003). Identifying the nature of the PKD-2 aggregates

Table 3. PKD-2::GFP neuronal distribution patterns in wild-type and mutant backgrounds

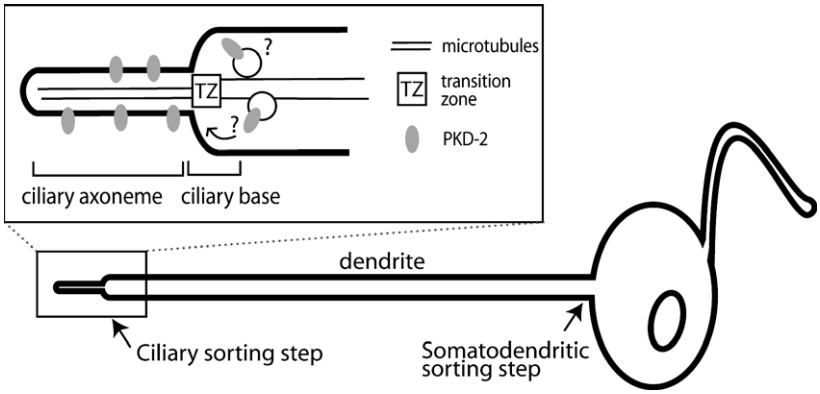

	Cilium	Dendrite	Cell body	Axon
Wild type	++	++ (puncta)	++	++
Non-native cell	–	–	++	–
unc-101	++	+++ (uniform)	++	+++ (uniform)
lov-1	+/++	++ (puncta)	+++ (large aggregates)	++
IFT mutants	+++	++ (puncta)	+/++	++

+, relatively reduced; ++, wild-type level; +++, relatively increased; –, not present.

in the *lov-1* mutant and determining whether this phenomenon occurs in ADPKD cells are important next steps in understanding TRPP2 trafficking.

The kinesin 3 KLP-6 is another cell-type specific factor regulating PKD-2 subcellular distribution (Peden and Barr, 2005). Mammalian kinesin 2/KIF3 (IFT kinesins) and kinesin 3/KIF16B (KLP-6) have been implicated in transporting endocytic organelles (Brown et al., 2005; Hoepfner et al., 2005). Interestingly, post-ER vesicles are found in ciliary bases of *pkd-2*-expressing neurons (Fig. 1D,E). In human respiratory epithelial cells, a *trans*-Golgi network marker localizes to ciliary bases (Schermer et al., 2005), implicating this region as an active protein turnover and trafficking site.

In both *klp-6* and IFT mutants, PKD-2 accumulates at the ciliary base and cilium, if formed. In contrast to IFT mutants, *klp-6* animals have superficially normal cilia, indicating that PKD-2 accumulation phenotype is not merely a consequence of ciliogenesis defects. Additionally, our data show that dendritic motility of PKD-2::GFP particles is not abrogated in various IFT and *klp-6* single mutants. Why then does PKD-2 accumulate in IFT and *klp-6* mutants? IFT and KLP-6 may somehow regulate PKD-2 abundance in cilia. In *Chlamydomonas*, flagellar turnover products are removed from flagella via retrograde IFT (Qin et al., 2004). IFT may play a similar role in the recycling of ciliary membrane receptors and signaling molecules. Ciliary abundance of PKD-2 is regulated by phosphorylation status, which is controlled by calcineurin and CK2 (Hu et al., 2006). Determining how the IFT process or IFT driven signaling molecules fit into this downregulation pathway will be informative.

Recent genomic and proteomic approaches have identified components required for formation and function of cilia and flagella (Avidor-Reiss et al., 2004; Blacque et al., 2005; Efimenko et al., 2005; Keller et al., 2005; Li et al., 2004; Ostrowski et al., 2002; Pazour et al., 2005). In contrast to ciliogenesis, very little is known regarding 'sensorigenesis', the process by which a cilium is specialized for a particular function. Cilia often possess unique morphologies and express a distinct repertoire of sensory receptors and signaling molecules. TRPP1 and TRPP2 are required for the flow-induced mechanosensory properties of kidney cilia (Nauli et al., 2003; Praetorius and Spring, 2001; Praetorius and Spring, 2003a; Praetorius and Spring, 2003b), with defects resulting in ADPKD. How is this essential polycystin sensory complex regulated? How is the renal primary cilium specified for sensing urine flow? Identification of general and tissue-specific pathways mediating ciliary protein localization and function are of utmost importance from both cell biology and human health perspectives.

We thank Shohei Mitani, Laurent Segelat and the Caenorhabditis Genetics Center (CGC) for strains; Alexander Van der Bliek for the GFP::KDEL marker (Labrousse et al., 1999); Jonathan Scholey for KAP-1::GFP; Andy Fire for *C. elegans* vectors; Doug Portman for the *tbb-4* cDNA; Erik Peden and Juan Wang for critical reading of this manuscript; John White for important experimental suggestions; Dave Saber for integration and behavioral assays; Doug Braun for excellent technical assistance; and the two anonymous reviewers for constructive criticism. This work was supported by the PKD Foundation and NIH.

References

Andrade, Y. N., Fernandes, J., Vazquez, E., Fernandez-Fernandez, J. M., Arniges, M., Sanchez, T. M., Villalon, M. and Valverde, M. A. (2005). TRPV4 channel is involved in the coupling of fluid viscosity changes to epithelial ciliary activity. *J. Cell Biol.* **168**, 869-874.

Ansley, S. J., Badano, J. L., Blacque, O. E., Hill, J., Hoskins, B. E., Leitch, C. C., Kim, J. C., Ross, A. J., Eichers, E. R., Teslovich, T. M. et al. (2003). Basal body dysfunction is a likely cause of pleiotropic Bardet-Biedl syndrome. *Nature* **425**, 628-633.

Avidor-Reiss, T., Maer, A. M., Koundakjian, E., Polyanovsky, A., Keil, T., Subramaniam, S. and Zuker, C. S. (2004). Decoding cilia function: defining specialized genes required for compartmentalized cilia biogenesis. *Cell* **117**, 527-539.

Barr, M. M. (2005). *Caenorhabditis elegans* as a model to study renal development and disease: sexy cilia. *J. Am. Soc. Nephrol.* **16**, 305-312.

Barr, M. M. and Sternberg, P. W. (1999). A polycystic kidney-disease gene homologue required for male mating behaviour in *C. elegans*. *Nature* **401**, 386-389.

Barr, M. M., DeModena, J., Braun, D., Nguyen, C. Q., Hall, D. H. and Sternberg, P. W. (2001). The *Caenorhabditis elegans* autosomal dominant polycystic kidney disease gene homologs *lov-1* and *pkd-2* act in the same pathway. *Curr. Biol.* **11**, 1341-1346.

Bell, L. R., Stone, S., Yochem, J., Shaw, J. E. and Herman, R. K. (2006). The molecular identities of the *Caenorhabditis elegans* intraflagellar transport genes *dyf-6*, *daf-10*, and *osm-1*. *Genetics* **173**, 1275-1286.

Blacque, O. E., Reardon, M. J., Li, C., McCarthy, J., Mahjoub, M. R., Ansley, S. J., Badano, J. L., Mah, A. K., Beales, P. L., Davidson, W. S. et al. (2004). Loss of *C. elegans* BBS-7 and BBS-8 protein function results in cilia defects and compromised intraflagellar transport. *Genes Dev.* **18**, 1630-1642.

Blacque, O. E., Perens, E. A., Boroevich, K. A., Inglis, P. N., Li, C., Warner, A., Khattra, J., Holt, R. A., Ou, G., Mah, A. K. et al. (2005). Functional genomics of the cilium, a sensory organelle. *Curr. Biol.* **15**, 935-941.

Bonifacino, J. S. and Traub, L. M. (2003). Signals for sorting of transmembrane proteins to endosomes and lysosomes. *Annu. Rev. Biochem.* **72**, 395-447.

Bredt, D. S. (1998). Sorting out genes that regulate epithelial and neuronal polarity. *Cell* **94**, 691-694.

Brenner, S. (1974). The genetics of *Caenorhabditis elegans*. *Genetics* **77**, 71-94.

Brodsky, F. M., Chen, C. Y., Knuehl, C., Towler, M. C. and Wakeham, D. E. (2001). Biological basket weaving: formation and function of clathrin-coated vesicles. *Annu. Rev. Cell Dev. Biol.* **17**, 517-568.

Brown, C. L., Maier, K. C., Stauber, T., Ginkel, L. M., Wordeman, L., Vernos, I. and Schroer, T. A. (2005). Kinesin-2 is a motor for late endosomes and lysosomes. *Traffic* **6**, 1114-1124.

Burbea, M., Dreier, L., Dittman, J. S., Grunwald, M. E. and Kaplan, J. M. (2002). Ubiquitin and AP180 regulate the abundance of GLR-1 glutamate receptors at postsynaptic elements in *C. elegans*. *Neuron* **35**, 107-120.

Clapham, D. E. (2003). TRP channels as cellular sensors. *Nature* **426**, 517-524.

Colbert, H. A., Smith, T. L. and Bargmann, C. I. (1997). OSM-9, a novel protein with structural similarity to channels, is required for olfaction, mechanosensation, and olfactory adaptation in *Caenorhabditis elegans*. *J. Neurosci.* **17**, 8259-8269.

Collet, J., Spike, C. A., Lundquist, E. A., Shaw, J. E. and Herman, R. K. (1998). Analysis of *osm-6*, a gene that affects sensory cilium structure and sensory neuron function in *Caenorhabditis elegans*. *Genetics* **148**, 187-200.

Deretic, D. and Papermaster, D. S. (1991). Polarized sorting of rhodopsin on post-Golgi membranes in frog retinal photoreceptor cells. *J. Cell Biol.* **113**, 1281-1293.

Dwyer, N. D., Troemel, E. R., Sengupta, P. and Bargmann, C. I. (1998). Odorant receptor localization to olfactory cilia is mediated by ODR-4, a novel membrane-associated protein. *Cell* **93**, 455-466.

Dwyer, N. D., Adler, C. E., Crump, J. G., L'Etoile, N. D. and Bargmann, C. I. (2001). Polarized dendritic transport and the AP-1 mu1 clathrin adaptor UNC-101 localize odorant receptors to olfactory cilia. *Neuron* **31**, 277-287.

Efimenko, E., Bubb, K., Mak, H. Y., Holzman, T., Leroux, M. R., Ruvkun, G., Thomas, J. H. and Swoboda, P. (2005). Analysis of *xbx* genes in *C. elegans*. *Development* **132**, 1923-1934.

Evans, J. E., Snow, J. J., Gunnarson, A. L., Ou, G., Stahlberg, H., McDonald, K. L. and Scholey, J. M. (2006). Functional modulation of IFT kinesins extends the sensory repertoire of ciliated neurons in *Caenorhabditis elegans*. *J. Cell Biol.* **172**, 663-669.

Geng, L., Okuhara, D., Yu, Z., Tian, X., Cai, Y., Shibazaki, S. and Somlo, S. (2006). Polycystin-2 traffics to cilia independently of polycystin-1 by using an N-terminal RVxP motif. *J. Cell Sci.* **119**, 1383-1395.

Gong, Z., Son, W., Chung, Y. D., Kim, J., Shin, D. W., McClung, C. A., Lee, Y., Lee, H. W., Chang, D. J., Kaang, B. K. et al. (2004). Two interdependent TRPV channel subunits, inactive and Nanchung, mediate hearing in *Drosophila*. *J. Neurosci.* **24**, 9059-9066.

Granato, M., Schnabel, H. and Schnabel, R. (1994). *pha-1*, a selectable marker for gene transfer in *C. elegans*. *Nucleic Acids Res.* **22**, 1762-1763.

Greenfield, J. J. and High, S. (1999). The Sec61 complex is located in both the ER and the ER-Golgi intermediate compartment. *J. Cell Sci.* **112**, 1477-1486.

Hanaoka, K., Qian, F., Boletta, A., Bhunia, A. K., Piontek, K., Tsiokas, L., Sukhatme, V. P., Guggino, W. B. and Germino, G. G. (2000). Co-assembly of polycystin-1 and -2 produces unique cation-permeable currents. *Nature* **408**, 990-994.

Haycraft, C. J., Schafer, J. C., Zhang, Q., Taulman, P. D. and Yoder, B. K. (2003). Identification of CHE-13, a novel intraflagellar transport protein required for cilia formation. *Exp. Cell Res.* **284**, 249-261.

Hodgkin, J. (1983). Male phenotypes and mating efficiency in *Caenorhabditis elegans*. *Genetics* **103**, 43-64.

Hoepfner, S., Severin, F., Cabezas, A., Habermann, B., Runge, A., Gillooly, D., Stenmark, H. and Zerial, M. (2005). Modulation of receptor recycling and degradation by the endosomal kinesin KIF16B. *Cell* **121**, 437-450.
Hu, J., Bae, Y. K., Knobel, K. M. and Barr, M. M. (2006). Casein kinase II and calcineurin modulate TRPP function and ciliary localization. *Mol. Biol. Cell* **172**, 663-669.
Hughes, J., Ward, C. J., Peral, B., Aspinwall, R., Clark, K., San Millan, J. L., Gamble, V. and Harris, P. C. (1995). The polycystic kidney disease 1 (PKD1) gene encodes a novel protein with multiple cell recognition domains. *Nat. Genet.* **10**, 151-160.
Igarashi, P. and Somlo, S. (2002). Genetics and pathogenesis of polycystic kidney disease. *J. Am. Soc. Nephrol.* **13**, 2384-2398.
Keller, L. C., Romijn, E. P., Zamora, I., Yates, J. R., 3rd and Marshall, W. F. (2005). Proteomic analysis of isolated *Chlamydomonas* centrioles reveals orthologs of ciliary-disease genes. *Curr. Biol.* **15**, 1090-1098.
Kim, J., Chung, Y. D., Park, D. Y., Choi, S., Shin, D. W., Soh, H., Lee, H. W., Son, W., Yim, J., Park, C. S. et al. (2003). A TRPV family ion channel required for hearing in *Drosophila*. *Nature* **424**, 81-84.
Kottgen, M., Benzing, T., Simmen, T., Tauber, R., Buchholz, B., Feliciangeli, S., Huber, T. B., Schermer, B., Kramer-Zucker, A., Hopker, K. et al. (2005). Trafficking of TRPP2 by PACS proteins represents a novel mechanism of ion channel regulation. *EMBO J.* **24**, 705-716.
Kozminski, K. G., Johnson, K. A., Forscher, P. and Rosenbaum, J. L. (1993). A motility in the eukaryotic flagellum unrelated to flagellar beating. *Proc. Natl. Acad. Sci. USA* **90**, 5519-5523.
Kozminski, K. G., Beech, P. L. and Rosenbaum, J. L. (1995). The *Chlamydomonas* kinesin-like protein FLA10 is involved in motility associated with the flagellar membrane. *J. Cell Biol.* **131**, 1517-1527.
Labrousse, A. M., Zappaterra, M. D., Rube, D. A. and van der Bliek, A. M. (1999). *C. elegans* dynamin-related protein DRP-1 controls severing of the mitochondrial outer membrane. *Mol. Cell* **4**, 815-826.
Li, J. B., Gerdes, J. M., Haycraft, C. J., Fan, Y., Teslovich, T. M., May-Simera, H., Li, H., Blacque, O. E., Li, L., Leitch, C. C. et al. (2004). Comparative genomics identifies a flagellar and basal body proteome that includes the BBS5 human disease gene. *Cell* **117**, 541-552.
Lints, R. and Emmons, S. W. (2002). Regulation of sex-specific differentiation and mating behavior in *C. elegans* by a new member of the DM domain transcription factor family. *Genes Dev.* **16**, 2390-2402.
Maduro, M. and Pilgrim, D. (1995). Identification and cloning of *unc-119*, a gene expressed in the *Caenorhabditis elegans* nervous system. *Genetics* **141**, 977-988.
Martin, E., Laloux, H., Couette, G., Alvarez, T., Bessou, C., Hauser, O., Sookhareea, S., Labouesse, M. and Segalat, L. (2002). Identification of 1088 new transposon insertions of *Caenorhabditis elegans*: a pilot study toward large-scale screens. *Genetics* **162**, 521-524.
Miller, M. S., Esparza, J. M., Lippa, A. M., Lux, F. G., 3rd, Cole, D. G. and Dutcher, S. K. (2005). Mutant kinesin-2 motor subunits increase chromosome loss. *Mol. Biol. Cell* **16**, 3810-3820.
Miyabayashi, T., Palfreyman, M. T., Sluder, A. E., Slack, F. and Sengupta, P. (1999). Expression and function of members of a divergent nuclear receptor family in *Caenorhabditis elegans*. *Dev. Biol.* **215**, 314-331.
Mochizuki, T., Wu, G., Hayashi, T., Xenophontos, S. L., Veldhuisen, B., Saris, J. J., Reynolds, D. M., Cai, Y., Gabow, P. A., Pierides, A. et al. (1996). *PKD2*, a gene for polycystic kidney disease that encodes an integral membrane protein. *Science* **272**, 1339-1342.
Nauli, S. M., Alenghat, F. J., Luo, Y., Williams, E., Vassilev, P., Li, X., Elia, A. E., Lu, W., Brown, E. M., Quinn, S. J. et al. (2003). Polycystins 1 and 2 mediate mechanosensation in the primary cilium of kidney cells. *Nat. Genet.* **33**, 129-137.
Nonet, M. L., Holgado, A. M., Brewer, F., Serpe, C. J., Norbeck, B. A., Holleran, J., Wei, L., Hartwieg, E., Jorgensen, E. M. and Alfonso, A. (1999). UNC-11, a *Caenorhabditis elegans* AP180 homologue, regulates the size and protein composition of synaptic vesicles. *Mol. Biol. Cell* **10**, 2343-2360.
Orozco, J. T., Wedaman, K. P., Signor, D., Brown, H., Rose, L. and Scholey, J. M. (1999). Movement of motor and cargo along cilia. *Nature* **398**, 674.
Ostrowski, L. E., Blackburn, K., Radde, K. M., Moyer, M. B., Schlatzer, D. M., Moseley, A. and Boucher, R. C. (2002). A proteomic analysis of human cilia: identification of novel components. *Mol. Cell Proteomics* **1**, 451-465.
Ou, G., Blacque, O. E., Snow, J. J., Leroux, M. R. and Scholey, J. M. (2005). Functional coordination of intraflagellar transport motors. *Nature* **436**, 583-587.
Pazour, G. J. (2004). Intraflagellar transport and cilia-dependent renal disease: the ciliary hypothesis of polycystic kidney disease. *J. Am. Soc. Nephrol.* **15**, 2528-2536.
Pazour, G. J. and Rosenbaum, J. L. (2002). Intraflagellar transport and cilia-dependent diseases. *Trends Cell Biol.* **12**, 551-555.
Pazour, G. J., San Agustin, J. T., Follit, J. A., Rosenbaum, J. L. and Witman, G. B. (2002). Polycystin-2 localizes to kidney cilia and the ciliary level is elevated in *orpk* mice with polycystic kidney disease. *Curr. Biol.* **12**, R378-R380.
Pazour, G. J., Agrin, N., Leszyk, J. and Witman, G. B. (2005). Proteomic analysis of a eukaryotic cilium. *J. Cell Biol.* **170**, 103-113.
Peden, E. M. and Barr, M. M. (2005). The KLP-6 kinesin is required for male mating behaviors and polycystin localization in *Caenorhabditis elegans*. *Curr. Biol.* **15**, 394-404.
Perkins, L. A., Hedgecock, E. M., Thomson, J. N. and Culotti, J. G. (1986). Mutant sensory cilia in the nematode *Caenorhabditis elegans*. *Dev. Biol.* **117**, 456-487.
Portman, D. S. and Emmons, S. W. (2004). Identification of *C. elegans* sensory ray genes using whole-genome expression profiling. *Dev. Biol.* **270**, 499-512.
Praetorius, H. A. and Spring, K. R. (2001). Bending the MDCK cell primary cilium increases intracellular calcium. *J. Membr. Biol.* **184**, 71-79.
Praetorius, H. A. and Spring, K. R. (2003a). Removal of the MDCK cell primary cilium abolishes flow sensing. *J. Membr. Biol.* **191**, 69-76.
Praetorius, H. A. and Spring, K. R. (2003b). The renal cell primary cilium functions as a flow sensor. *Curr. Opin. Nephrol. Hypertens.* **12**, 517-520.
Qin, H., Rosenbaum, J. L. and Barr, M. M. (2001). An autosomal recessive polycystic kidney disease gene homolog is involved in intraflagellar transport in *C. elegans* ciliated sensory neurons. *Curr. Biol.* **11**, 457-461.
Qin, H., Diener, D. R., Geimer, S., Cole, D. G. and Rosenbaum, J. L. (2004). Intraflagellar transport (IFT) cargo: IFT transports flagellar precursors to the tip and turnover products to the cell body. *J. Cell Biol.* **164**, 255-266.
Qin, H., Burnette, D. T., Bae, Y.-K., Forscher, P., Barr, M. M. and Rosenbaum, J. L. (2005). Intraflagellar transport is required for the vectorial movement of TRPV channels in the ciliary membrane. *Curr. Biol.* **15**, 1695-1699.
Reboul, J., Vaglio, P., Rual, J. F., Lamesch, P., Martinez, M., Armstrong, C. M., Li, S., Jacotot, L., Bertin, N., Janky, R. et al. (2003). *C. elegans* ORFeome version 1.1: experimental verification of the genome annotation and resource for proteome-scale protein expression. *Nat. Genet.* **34**, 35-41.
Rosenbaum, J. L. and Witman, G. B. (2002). Intraflagellar transport. *Nat. Rev. Mol. Cell Biol.* **3**, 813-825.
Schermer, B., Hopker, K., Omran, H., Ghenoiu, C., Fliegauf, M., Fekete, A., Horvath, J., Kottgen, M., Hackl, M., Zschiedrich, S. et al. (2005). Phosphorylation by casein kinase 2 induces PACS-1 binding of nephrocystin and targeting to cilia. *EMBO J.* **24**, 4415-4424.
Sengupta, P., Chou, J. H. and Bargmann, C. I. (1996). *odr-10* encodes a seven transmembrane domain olfactory receptor required for responses to the odorant diacetyl. *Cell* **84**, 899-909.
Shakir, M. A., Fukushige, T., Yasuda, H., Miwa, J. and Siddiqui, S. S. (1993). *C. elegans* osm-3 gene mediating osmotic avoidance behaviour encodes a kinesin-like protein. *NeuroReport* **4**, 891-894.
Shim, J., Sternberg, P. W. and Lee, J. (2000). Distinct and redundant functions of mu1 medium chains of the AP-1 clathrin-associated protein complex in the nematode *Caenorhabditis elegans*. *Mol. Biol. Cell* **11**, 2743-2756.
Signor, D., Wedaman, K. P., Orozco, J. T., Dwyer, N. D., Bargmann, C. I., Rose, L. S. and Scholey, J. M. (1999a). Role of a class DHC1b dynein in retrograde transport of IFT motors and IFT raft particles along cilia, but not dendrites, in chemosensory neurons of living *Caenorhabditis elegans*. *J. Cell Biol.* **147**, 519-530.
Signor, D., Wedaman, K. P., Rose, L. S. and Scholey, J. M. (1999b). Two heteromeric kinesin complexes in chemosensory neurons and sensory cilia of *Caenorhabditis elegans*. *Mol. Biol. Cell* **10**, 345-360.
Snow, J. J., Ou, G., Gunnarson, A. L., Walker, M. R., Zhou, H. M., Brust-Mascher, I. and Scholey, J. M. (2004). Two anterograde intraflagellar transport motors cooperate to build sensory cilia on *C. elegans* neurons. *Nat. Cell Biol.* **6**, 1109-1113.
Sulston, J. E., Albertson, D. G. and Thomson, J. N. (1980). The *Caenorhabditis elegans* male: postembryonic development of nongonadal structures. *Dev. Biol.* **78**, 542-576.
Terasaki, M., Jaffe, L. A., Hunnicutt, G. R. and Hammer, J. A., 3rd (1996). Structural change of the endoplasmic reticulum during fertilization: evidence for loss of membrane continuity using the green fluorescent protein. *Dev. Biol.* **179**, 320-328.
Tobin, D., Madsen, D., Kahn-Kirby, A., Peckol, E., Moulder, G., Barstead, R., Maricq, A. and Bargmann, C. (2002). Combinatorial expression of TRPV channel proteins defines their sensory functions and subcellular localization in *C. elegans* neurons. *Neuron* **35**, 307-318.
Ward, S., Thomson, N., White, J. G. and Brenner, S. (1975). Electron microscopical reconstruction of the anterior sensory anatomy of the nematode *Caenorhabditis elegans*. *J. Comp. Neurol.* **160**, 313-337.
Watnick, T. and Germino, G. (2003). From cilia to cyst. *Nat. Genet.* **34**, 355-356.
Wicks, S. R., de Vries, C. J., van Luenen, H. G. and Plasterk, R. H. (2000). CHE-3, a cytosolic dynein heavy chain, is required for sensory cilia structure and function in *Caenorhabditis elegans*. *Dev. Biol.* **221**, 295-307.
Yoder, B. K., Hou, X. and Guay-Woodford, L. M. (2002). The polycystic kidney disease proteins, polycystin-1, polycystin-2, polaris, and cystin, are co-localized in renal cilia. *J. Am. Soc. Nephrol.* **13**, 2508-2516.